

Pulse interval tunable terahertz radiation from electron beam-plasma interactions

Die Jian(简蝶), Jie Cai(蔡杰), Li-Qi Han(韩立琦), Xing-Yu Zhao(赵兴宇), Han Wen(温寒), and Jin-Qing Yu(余金清)
Citation: Chin. Phys. B, 2025, 34 (**10**): 105201. DOI: 10.1088/1674-1056/add67a
http://cpb.iphy.ac.cn; http://iopscience.iop.org/cpb

What follows is a list of articles you may be interested in

Simulation of capacitively coupled Ar/O_2 discharges based on global/equivalent circuit model and an extended reaction set

Yi Wang(王怡), Wan Dong(董婉), Yi-Fan Zhang(张逸凡), Liu-Qin Song(宋柳琴), and Yuan-Hong Song(宋远红)
Chin. Phys. B, 2025, 34 (**8**): 085201. DOI: 10.1088/1674-1056/add4e5

Effect of gold doping on relativistic electron beam transport in high-density plasma

Zi-Yan Zhang(张子彦) and Wei-Min Wang(王伟民)
Chin. Phys. B, 2025, 34 (**7**): 075201. DOI: 10.1088/1674-1056/add4df

Discharge mode and particle transport in radio frequency capacitively coupled Ar/O_2 plasma discharges

Zhuo-Yao Gao(高卓瑶), Wan Dong(董婉), Chong-Biao Tian(田崇彪), Xing-Zhao Jiang(蒋星照), Zhong-Ling Dai(戴忠玲), and Yuan-Hong Song(宋远红)
Chin. Phys. B, 2024, 33 (**9**): 095203. DOI: 10.1088/1674-1056/ad5d65

Power transfer efficiency in an air-breathing radio frequency ion thruster

Gao-Huang Huang(黄高煌), Hong Li(李宏), Fei Gao(高飞), and You-Nian Wang(王友年)
Chin. Phys. B, 2024, 33 (**7**): 075201. DOI: 10.1088/1674-1056/ad426c

Effects of diamagnetic drift on nonlinear interaction between multi-helicity neoclassical tearing modes

Haiyuan Wang(王海源), Shuai Jiang(姜帅), Tong Liu(刘桐), Lai Wei(魏来), Qibin Luan(栾其斌), and Zheng-Xiong Wang(王正汹)
Chin. Phys. B, 2024, 33 (**6**): 065202. DOI: 10.1088/1674-1056/ad24d3

Pulse interval tunable terahertz radiation from electron beam–plasma interactions

Die Jian(简蝶)[1], Jie Cai(蔡杰)[2], Li-Qi Han(韩立琦)[1], Xing-Yu Zhao(赵兴宇)[1], Han Wen(温寒)[1,†], and Jin-Qing Yu(余金清)[1]

[1] *Hunan Provincial Key Laboratory of High-Energy Scale Physics and Applications, School of Physics and Electronics, Hunan University, Changsha* 410082, *China*

[2] *State Key Laboratory of Nuclear Physics and Technology, Key Laboratory of HEDP of the Ministry of Education, CAPT, Peking University, Beijing* 100871, *China*

(Received 19 March 2025; revised manuscript received 24 April 2025; accepted manuscript online 9 May 2025)

Terahertz (THz) radiation is rapidly emerging as a powerful tool with diverse applications, including high-speed imaging, laser-driven particle acceleration, and ultra-high frequency (UHF) communications. However, generating multi-pulse THz radiation with controllable time intervals remains a significant challenge. This study presents an approach to overcome this hurdle by exploiting the interaction between an electron beam and plasma. Using numerical simulations and theoretical analysis, we investigated the behavior of an electron beam within a plasma and its interaction with the longitudinal sheath field. This interaction resulted in the generation of multiple distinct THz pulses. We demonstrated that the plasma length adjustment allows for precise tuning of the interval between THz pulses. Moreover, the radiation intensity could be controlled by the electron beam energy and the electron bunch duration. The proposed scheme can generate multi-pulse THz radiation in a flexible and precise manner, paving the way for advancements in applications requiring high temporal resolution.

Keywords: electron beam, plasma, terahertz, particle-in-cell simulation

PACS: 52.40.Mj, 52.59.–f, 52.65.Rr, 52.25.Os

DOI: 10.1088/1674-1056/add67a **CSTR:** 32038.14.CPB.add67a

1. Introduction

Terahertz (THz) radiation,[1] occupying the spectral range of 0.1 THz–10 THz,[2] exhibits distinctive properties including high penetration depth, low radiation loss, and non-destructive interaction with biological tissues and materials.[3] These unique characteristics have driven significant interest in THz technologies for diverse applications such as material characterization,[4] time-domain spectroscopy,[5] next-generation wireless communications,[6,7] non-destructive evaluation,[8] and biomedical imaging.[9,10] The growing demand for THz applications has stimulated substantial progress in plasma-based THz generation mechanisms.[11] Current approaches include linear mode conversion,[12] two-color laser schemes,[13] coherent transition radiation,[14,15] and plasma waveguide configurations.[16] A recent breakthrough in electron beam manipulation[17] presents new opportunities for THz generation. Research into THz sources is currently focused on the generation and optimization of single-pulse radiation. For example, Simpson *et al.* proposed a novel optical configuration that produced a single-cycle THz pulse with high coherence and excellent directionality.[18] However, this method relies on complex optics and demanding experimental conditions, increasing the complexity and cost of the system. In contrast, plasma-based direct generation methods offer a much cleaner and more efficient route for THz generation. For example, fast electron beams with a duration of femtosecond (fs) can interact with plasmas and emit THz radiation. Such setup was demonstrated in the relativistic laser–foil interaction experiments.[19] Notably, the observed THz signals are not single pulses but consist of temporally separated bursts, indicating a distinct multi-pulse structure. In recent years, the generation and control of multi-pulse THz radiation have attracted increasing attention, with its underlying mechanisms investigated through analytical theory[20] and numerical simulations.[21,22]

The investigation of plasma source configurations for efficient multi-pulse THz generation remains a critical research frontier, a challenge compounded by the complex dynamics of electron motion in plasma. High-energy electron interactions with plasma surfaces can generate radiations through multiple mechanisms,[22] namely, transition radiation (TR),[23] bremsstrahlung-like radiation (BR),[24] and sheath radiation (SR).[25,26] Transition radiation occurs when a charge particle crosses the boundary of two types of materials with different dielectric constants.[27] In the context of interactions between electron beams and plasmas, TR originates from the dielectric contrast at the plasma–vacuum interfaces.[28,29] Concurrently, transient charge imbalance at the plasma boundary establishes

†Corresponding author. E-mail: hwen@hnu.edu.cn

© 2025 Chinese Physical Society and IOP Publishing Ltd. All rights, including for text and data mining, AI training, and similar technologies, are reserved.

intense electrostatic sheath fields[30] that cause surface atom ionization, ion acceleration, and low-energy electron recirculation into the plasma.[31,32] The sheath fields induce complex electron trajectories, including deceleration, acceleration, and the repeated exiting and reentering of electrons into the target, which give rise to transient emissions collectively referred to as bremsstrahlung-like transition radiation (bTR).[19,33] Notably, sheath charge dissipation generates transient longitudinal currents responsible for SR emission.[26,34–36] Although understanding these coupled mechanisms is fundamental for advancing the field of THz generation, there is no clear path to achieving precisely control over temporal pulse separation using these mechanisms alone.

In this work, we present a theoretical framework for generating THz radiation through an electron beam-driven ultrashort plasma mechanism.[37] This approach enables multi-pulse THz emission with tunable temporal intervals, thereby expanding the design space for THz sources and creating new opportunities for advanced applications. Through comprehensive phase-space analysis of plasma electron dynamics, we characterized the underlying electron trajectories and radiation mechanisms while validating this model through first-principles particle-in-cell (PIC) simulations.

2. Scheme and electron kinetics

The schematic diagram of the multi-pulse THz scheme is illustrated in Fig. 1(a). When a relativistic electron beam irradiates on a plasma slab along one of the symmetric axes, it simultaneously generates THz radiation[38] and establishes a longitudinal sheath field.[39] The longitudinal electrostatic sheath fields at the plasma boundaries drive periodic electron beam oscillations within the plasma, enabling sequential multi-pulse generation.[37] As demonstrated by Cai *et al.*,[37] this sheath field mediates two distinct electron behaviors: high-energy electrons overcome the potential barrier and escape the plasma boundary, while lower-energy electrons become trapped and recirculate within the plasma bulk.[31] The confined electrons undergo periodic sheath-driven oscillations across the plasma interface, generating coherent electromagnetic radiation through recurrent acceleration–deceleration cycles, particularly in the THz regime. This oscillatory motion exhibits similarities to the betatron resonance mechanisms, where sheath field interactions induce transient radiation analogous to bremsstrahlung processes.[24] The proposed scheme achieves multi-pulse THz generation through sheath-mediated electron confinement, independent of specific radiation mechanisms for individual pulses.

To investigate the detailed electron dynamics in plasma and associated radiation mechanisms, we performed kinetic simulations of electron–plasma interactions. An electron beam was initialized on the left side of the plasma and propagated along the x-axis to the right as shown in Fig. 1(a). The description of the exact parameters of the simulation are deferred to Section 3. Here we describe the typical electron dynamics to illustrate the general behaviors of the electron beam and the resulting radiations.

Three typical electrons with similar initial positions but different initial momenta were selected and their trajectory in the p_x–x phase space is shown in Fig. 1(b). Notably, despite the differences in their initial momenta, the momentum of the electrons decreases almost immediately once they started moving inside the plasma, with all electrons reaching the boundary nearly the same time. One can see from Fig. 1(b) that the electron momentum p_x underwent considerable changes during the first 15 μm of propagation. The strong longitudinal sheath field present at the boundary exerted a substantial influence on the electrons when they approached the boundary of the plasma, leading to the deceleration and acceleration of the electrons as indicated by the p_x sign change near the plasma boundaries (the two black dashed lines). Later on, the electrons moved periodically within the plasma, as shown by the oval-shaped trajectories in Fig. 1(b). There was small changes in electron momentum amplitude $|p_x|$ when electrons moved along the x-direction within one pass of the plasma, as indicated by the almost horizontal trajectories between the plasma boundaries. On the other hand, $|p_x|$ gradually diminishes over multiple passes. As evident in Fig. 1(b), the electrons with the largest p_x did not end up covering the longest distance, which suggests that the accumulated changes in $|p_x|$ are different for different electrons.

From the time evolution of the electron momentum depicted in Fig. 1(c), one can identify that the specific times at which the electrons reached either ends of the plasma by locating the rapid change in the electron momentum. Figure 1(c) shows that p_x decreased rapidly from a positive to a negative value at $t \approx 0.33$ ps. At this moment, the electron reached the right boundary of the plasma, where it was subjected to a positive longitudinal sheath field E_x as shown in Fig. 1(d). This field exerted a force opposite to the electron's motion, causing the electron to decelerate and then accelerate towards the negative x-direction. As the electron continued to traverse the plasma, it reached the left boundary of the plasma and encountered a negative longitudinal sheath field E_x at $t \approx 0.8$ ps. This field reversed the direction of the electron velocity, sending the electron towards the right boundary and completing one cycle of the periodic motion. It is worth noting that the electrons were not experiencing high fields except when near the boundaries as apparent in Fig. 1(d). Therefore, the radiation intensity is expected to peak when the electrons cross the plasma boundary and decrease to low levels once the electrons start coasting inside the plasma. This sheath-driven periodic mo-

tion can generate recurring THz pulses by repeating boundary crossings as long as the boundary-crossing time is small compared to the plasma-traverse time. However, progressive phase decoupling emerges over time. While initial oscillations maintain high temporal coherence, gradual momentum-dependent damping disrupts the synchronized boundary crossings. As shown in Fig. 1(c), the once-synchronized electrons became out-of-sync round $t \approx 2$ ps, effectively making the boundary-crossing time for the electron beam longer and longer. Eventually, as the electron beam spreads throughout the plasma, the plasma can no longer generate discernible THz pulses. Our analysis confirmed that the longitudinal sheath field governed the electron confinement and oscillation that are essential for multi-pulse THz emission.

The electron energy density as a function of time further confirms the periodic oscillation of electrons within the plasma, as shown in Fig. 1(e). The longitudinal periodic motion of the electrons directly leads to a distinct step-like change in the energy distribution. When the electron beam oscillates to the boundary of the plasma, the number of high-energy electrons decreases, resulting in the electron beam energy dropping by one step and gradually dissipating into the low-energy region. As the oscillations continue, the step-like changes become increasingly blurred, indicating that the timing of the electrons reaching the plasma boundary becomes progressively unsynchronized. This process is consistent with the observed trend of decreasing amplitude of momentum oscillations in Fig. 1(c), indicating that over time, the electron motion gradually loses its regularity.

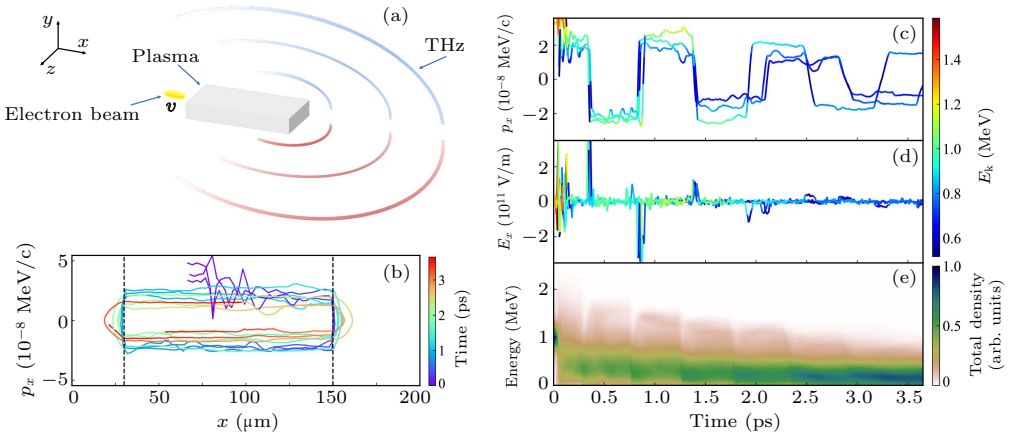


Fig. 1. (a) Schematic diagram of multi-pulse THz generation via electron beam–plasma interaction. An electron beam (yellow) with an initial energy of 1 MeV propagates into a 120 μm×30 μm plasma slab, generating coherent THz emission (red and blue waveforms) at the plasma–vacuum interface. A circular receiver screen with a radius of 250 μm is centered at the right boundary of the plasma to capture the emitted radiation. (b) Trajectories of confined electrons in phasespace: spatial coordinate X versus longitudinal momentum p_x. Two vertical dashed lines at $x = 30$ μm and $x = 150$ μm corresponds to the longitudinal boundaries of the plasma. (c) Time evolution of the electron momentum p_x. (d) Time evolution of the longitudinal sheath field E_x perceived by the electron. (e) Time evolution of the electron energy distribution. Panels (c), (d), and (e) share the same time axis.

As the general characteristic of the electron dynamics suggests, the interaction between the electron beam and the longitudinal sheath field at plasma boundaries is responsible for the intense THz generation while a small amount of energy is lost during the electrons propagation between the boundaries. This observation indicates the possibility of controlling the temporal interval of multi-pulse THz radiation by varying the plasma length.

3. Generation of multi-pulse terahertz radiation

To investigate the physical mechanisms underlying THz radiation generation, we conducted a series of two-dimensional (2D) PIC simulations[40] using the SMILEI code.[41] The simulation window spanned $X \times Y = 430.08\ \mu\text{m} \times 573.44\ \mu\text{m}$ and was divided into 8960×7168 cells. An electron beam was injected from the left boundary, propagating along the positive X-axis into a block-shaped plasma with adjustable length and thickness. The electron density of the electron beam is $n_e = 1.74 \times 10^{22}\ \text{m}^{-3}$. The electron beam had an energy spread of 57%, a pulse duration of 100 fs, and an angular divergence of 2.5°. A similar set of beam parameters can be achieved via laser wakefield acceleration.[42,43] Since the longitudinal sheath-driven oscillations significantly increase the divergence angle, the initial angle has no impact on the pulse interval or THz frequency as long as it does not exceed the divergence angle reached after the first oscillation. The electron density in the plasma is $n_0 = 3.489 \times 10^{26}\ \text{m}^{-3}$. Each cell was initialized with 2 macroparticles of ions (C^{6+}) and 100 macroparticles of electrons, forming a neutral background plasma. The experimental generation of the required plasma slab has been demonstrated in recent studies utilizing carbon nanotube foams.[44–46] Analysis of the simulations indicates that the electron beam generates concentrated radiation primarily at the plasma boundaries, with the most intense THz emission occurring at the right boundary due to the initial propagation direction of the beam. To effectively capture the radiation signal, a semi-circular receiver screen with a radius of 250 μm was placed on the right side of the plasma, centering at the transverse midpoint of the

right boundary. This configuration minimizes signal loss by collecting all electromagnetic waves propagating to the right. To capture the entire THz radiation generation process, the simulation time was adjusted based on the plasma length l_p, ensuring a duration of more than 1 ps. This duration is sufficient to capture the full evolution of the THz source and allows a detailed analysis of the underlying dynamics.

Figure 2(a) shows the THz signals collected by the receiver screen in the simulation results with the plasma length $l_p = 120$ μm and thickness $l_t = 30$ μm. One can observe three THz radiation pulses with progressively decreasing radiation intensities. The signals between the three main pulses correspond to the THz radiations generated inside and at the left boundary of the plasma. Additionally, the electric field distribution of the THz radiation exhibited significant directional characteristics. To further investigate this directional effect, we extracted the time-domain signals at three observation angles ($\theta = 50°$, $60°$, and $70°$, where θ is the angle between the radiation propagation direction and the positive X-direction) and applied a fast Fourier transform (FFT) to obtain the frequency spectrum. The spectrum was processed using a super-Gaussian low-pass filter with a cut-off frequency of 7 THz, as shown in Fig. 2(b). The bunch duration controls the high-frequency limit of the spectrum,[47] while the plasma length governs the central frequency through the oscillation dynamics. One can see that as the observation angle increases, the signal strength at frequencies above 3 THz gradually decreases. Moreover, the radiation was mainly concentrated in the low-frequency region (0 THz–4 THz) which corresponded to the fundamental frequency of the individual THz pulse.

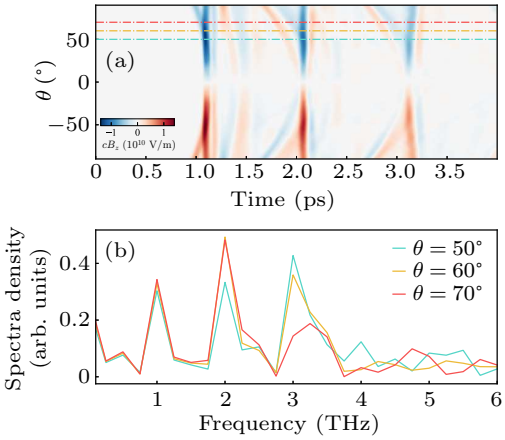


Fig. 2. (a) Angular distribution of the THz radiation electric field cB_z captured by the receiver screen. The dashed lines correspond to observation angles $\theta = 50°, 60°, 70°$. (b) Frequency spectrum of the THz signals that correspond to the lineouts in panel (a). The spectral density was normalized to the same arbitrary units.

Many multi-pulse THz applications require even temporal separations between pulses. The temporal evolution of the pulses was analyzed using the data at observation angle $\theta = 70°$ as an example. As shown in Fig. 3(a), three distinct pulses were observed at $t \approx 1.09$ ps, $t \approx 2.06$ ps, and $t \approx 3.14$ ps. The temporal separation between the second and third pulses is about 10% larger than that between the first and second pulses. This small temporal variation can be attributed to the energy loss induced by the THz radiation near the plasma boundaries. The accumulative beam–plasma interactions may also contribute to the slowing down of the electron beam: when propagating in the X-direction, the electrons also bounce between the plasma boundaries in the Y-direction, generating radiations and losing energy gradually along the way. The successively decreasing peak intensities and broadening peak widths are also clearly visible in Fig. 3(a), which are likely caused by the slowing-down, broadening, and divergence of the electron beam.

One can identify the time when the center of the electron beam reached the edge of the plasma by looking for the sudden decrease in total energy of the electron beam. The time evolution of the total energy of the electron beam is shown in Fig. 3(b). The first three times when the electron beam reached the right edge of the plasma were indicated by the vertical black lines, which corresponds to $t \approx 0.33$ ps, $t \approx 1.30$ ps, and $t \approx 2.38$ ps. Comparing these instants with the corresponding THz pulses recorded on the receiver screen, it can be seen that after each electron beam interaction with the right edge of the plasma, a significant THz pulse is detected by the receiver screen approximately 0.76 ps later, which agrees well with the propagation time for the radiation to travel from the right edge of the plasma to the receiver screen. The generation of these pulses is dominated by the transient processes during the interaction between the electron beam and the plasma boundary. By simultaneously reducing the electron bunch duration and the plasma length, the electrons can undergo more oscillations without significant divergence, thereby generating more THz pulses.

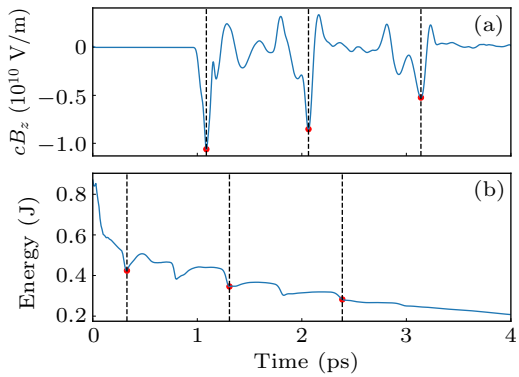


Fig. 3. (a) The time domain signal of the electric field cB_z corresponding to $\theta = 70°$ over time. (b) The evolution of the total driving electron beam energy over time.

4. Discussion

The temporal interval between THz pulses t_d, defined as the peak-to-peak time difference, can be adjusted by varying the plasma length l_p. To obtain the correlation between t_d and l_p, a parameter scan on l_p from 40 μm to 140 μm was performed using the PIC simulations. The plasma thickness was

kept constant at 30 μm and other parameters were the same as listed in Section 3. Figure 4(a) shows the time history of cB_z collected at $\theta = 50^\circ$ from three simulations with different values of l_p. The shape of the pulses remains largely unchanged as the plasma length increases. The energy partition of the main pulses (defined as 0.1 ps before and after each peak) relative to the total radiation energy was quantified using the data shown in Fig. 4(a). The results showed that the three main pulses accounted for about 85% of the total radiation energy regardless of the plasma lengths. It suggests that the fundamental mechanism producing terahertz pulses remains consistent regardless of the plasma length.

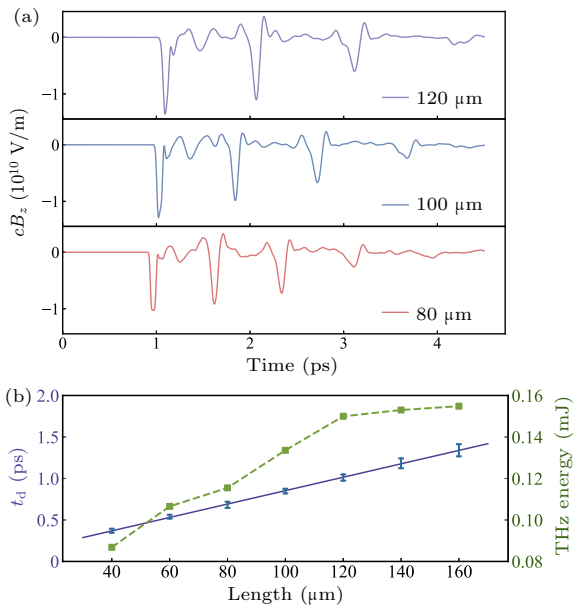


Fig. 4. (a) Time variation curves of the terahertz electric field cB_z for different plasma lengths ($l_p = 80$ μm, 100 μm, 120 μm). (b) Temporal interval between successive pulses (blue dots with error bars) together with its linear fit (purple line), and the THz radiation energy in the frequency range of 0.1 THz–6 THz (green dashed line), plotted as functions of plasma length.

Through linear regression analysis of pulse arrival times with different plasma lengths, a linear correlation between t_d and the plasma length l_p was found, as illustrated in Fig. 4(b). Using a simple physics model, the relation between t_d and l_p can be expressed as

$$t_d = \frac{2l_p}{v_b} + t_s, \tag{1}$$

where v_b denotes the velocity of the electron beam and t_s corresponds to the time of electron interactions near the plasma boundaries. The electron velocity $v_b \approx 2.47 \times 10^8$ m/s obtained by fitting agrees well with the velocity corresponding to 1-MeV electrons used in the simulations. The value of t_s obtained from fitting is 0.047 ps that is consistent with the width of the main pulses of the THz radiation.

The radiant energy of the THz signals collected from the receiver screen is shown in Fig. 4(b) as a function of l_p. Given the nature of the 2D simulations, both the plasma and the THz radiation were assumed to be uniform in the third dimension. The energy flux density method[48] was used to calculate the radiant energy for different plasma lengths. While the total radiation energy does not follow an obvious trend as l_p changes, the larger l_p leads to higher radiation energy in the range of 0.1 THz to 6 THz as shown in Fig. 4(b). The time of beam–plasma interactions inside the plasma becomes longer as l_p increases. This extended interaction increases the duration of the electron beam, which subsequently shifts the radiation spectrum towards lower frequencies through the TR processes.[24] We repeated the simulations with extended plasma lengths and observed that the THz energy increases with l_p up to approximately 160 μm, beyond which it saturates. The saturation is caused by the decrease in electron density n_e during transport, which leads to a reduction in the sheath field strength E_x for longer plasma targets.[37]

The influences of the electron beam energy and the thickness of the plasma were quantified with a parameter scan. All simulations were based on the simulation with $l_p = 80$ μm. Other common parameters were listed in Section 3. The scaling of the energy is shown in Fig. 5(a). Higher electron beam energy provides more energy for radiation, thereby increasing THz radiation intensity. A linear correlation was found for electron beam energy between 1 MeV and 3 MeV. However, the differences in pulse time intervals generated by varying electron beam energies are minimal (within 0.05 ps) because the energy of a relativistic electron beam is a strong function of the electron velocity. Changes in electron beam energy mainly affect the radiation intensity but not the beam velocity. As a result, changing the electron beam energy has little impact on the temporal interval t_d. Variations in thickness primarily affect the transverse sheath field distribution, which influences the transverse motion but not longitudinal motion of the electron beam. The mechanism proposed here mainly relies on the electron dynamics in the longitudinal direction. As a result, a change in thickness from 20 μm to 40 μm, or doubling the thickness, only causes 38% changes in the radiation energy. At the same time, the value of t_d only change by 0.01 ps, i.e., less than 2%. The linear scaling between THz energy and the plasma thickness could be attributed to the structure of the sheath fields at the plasma boundaries. Given the relatively small effects, such hypothesis will be left for future studies.

We scanned electron beams with different bunch duration from 5 μm to 125 μm as shown in Fig. 5(b). The saturation and subsequent decline in THz radiation energy as the electron duration length increases are primarily governed by the space-charge effect[49] and the loss of coherence.[49–51] Although the electron bunch duration affects the timing of the first pulse, it has little influence on the pulse interval. This is because the bunch rapidly broadens during the oscillation process and eventually expands to a length comparable to the

plasma target.

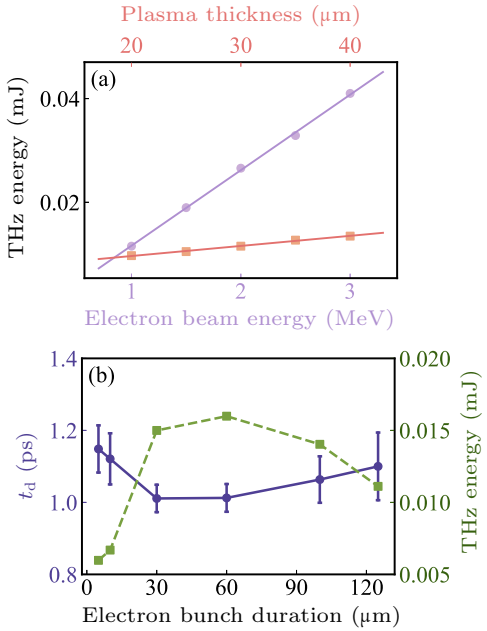


Fig. 5. (a) The dependence of the THz radiation energy on the electron beam energy (purple dots) and the thickness of the plasma (red squares). The linear fitting is plotted as solid lines with respective colors. (b) Temporal interval between successive pulses (purple dots with error bars) together with its linear fit (purple line), and the THz radiation energy in the frequency range of 0.1 THz–6 THz (green dashed line), plotted as functions of electron bunch duration.

5. Conclusion

Leveraging the interaction between an electron beam and a plasma, this study introduces a scheme for generating multi-pulse THz radiation. The kinetic behavior of the electron beam within the plasma and at its boundaries lead to the emission of three distinct THz pulses when a 1-MeV electron beam is injected into a plasma ($l_p = 120$ μm, $l_t = 30$ μm). Numerical simulations revealed that the temporal interval between THz pulses could be precisely controlled by varying the plasma length, while both the electron beam energy and bunch length strongly affect the radiation intensity and total THz energy. These findings offer a theoretical foundation for experimental validation and practical applications. These features make the scheme particularly promising for high-resolution THz applications, where controllability and pulse clarity are essential.

Acknowledgements

Project supported by the National Natural Science Foundation of China (Grant No. 12175058) and the National Science Fund of Hunan Province for Distinguished Young Scholars (Grant No. 2024JJ2009).

References

[1] Siegel P H 2002 *IEEE Transactions on microwave theory and techniques* **50** 910
[2] Dragoman D and Dragoman M 2004 *Progress in Quantum Electronics* **28** 1
[3] Pawar A Y, Sonawane D D, Erande K B and Derle D V 2013 *Drug Invention Today* **5** 157
[4] Kampfrath T, Tanaka K and Nelson K A 2013 *Nat. Photon.* **7** 680
[5] Jepsen P U, Cooke D G and Koch M 2011 *Laser Photon. Rev.* **5** 124
[6] Jiang W, Zhou Q, He J, Habibi M A, Melnyk S, El-Absi M, Han B, Renzo M D, Schotten H D, Luo F L, El-Bawab T S, Juntti M, Debbah M and Leung V C M 2024 *IEEE Communications Surveys & Tutorials* **26** 2326
[7] Xue Q, Ji C, Ma S, Guo J, Xu Y, Chen Q and Zhang W 2024 *IEEE Communications Surveys & Tutorials* **26** 1520
[8] Choi W J, Cheng G, Huang Z, Zhang S, Norris T B and Kotov N A 2019 *Nature Materials* **18** 820
[9] Oh S J, Kim S H, Ji Y B, Jeong K, Park Y, Yang J, Park D W, Noh S K, Kang S G, Huh Y M, *et al.* 2014 *Biomedical Optics Express* **5** 2837
[10] Pickwell E and Wallace V 2006 *J. Phys. D: Appl. Phys.* **39** R301
[11] Hamster H, Sullivan A, Gordon S, White W and Falcone R 1993 *Phys. Rev. Lett.* **71** 2725
[12] Liao G, Li Y, Li C, Su L, Zheng Y, Liu M, Wang W, Hu Z, Yan W, Dunn J, *et al.* 2015 *Phys. Rev. Lett.* **114** 255001
[13] Wang Y X, Shou Y R, Cai J, Han L Q, Geng Y X, Yu J Q and Yan X Q 2024 *Phys. Plasmas* **31** 033111
[14] Wu Z, Fisher A S, Goodfellow J, Fuchs M, Daranciang D, Hogan M, Loos H and Lindenberg A 2013 *Rev. Sci. Instrum.* **84** 022701
[15] Cai J, Shou Y, Han L, Huang R, Wang Y, Song Z, Geng Y, Yu J and Yan X 2022 *Opt. Lett.* **47** 1658
[16] Kahaly S, Yadav S, Wang W, Sengupta S, Sheng Z, Das f A, Kaw P and Kumar G R 2008 *Phys. Rev. Lett.* **101** 145001
[17] Liang Y, Liu Z, Tian Q, Li T, Lin X, Yan L, Du Y, Li R, Shi J, Cheng C, *et al.* 2023 *Nat. Photon.* **17** 259
[18] Simpson T T, Pigeon J J, Miller K G, Ramsey D, Froula D H and Palastro J P 2024 *Sci. Rep.* **14** 26587
[19] Liao G, Sun F, Lei H, Wang T, Wang D, Wei Y, Liu F, Wang X, Li Y and Zhang J 2024 *Phys. Rev. Lett.* **132** 155001
[20] Ding W, Li F, Weng S, Bai P and Sheng Z 2019 arXiv preprint arXiv: 1902.04716
[21] Wang J, Zhang Z, Zhou S, Qin Z, Yu C, Cao Y, Lv Y, Chen J, Huang H, Liu W, *et al.* 2025 *Laser Photon. Rev.* **19** 2400954
[22] Denoual E, Bergé L, Davoine X and Gremillet L 2023 *Phys. Rev. E* **108** 065211
[23] Gorlova D A, Tsymbalov I N, Tsygvintsev I P and Savelev A B 2024 *Laser Phys. Lett.* **21** 035001
[24] Liao G Q, Liu H, Scott G G, Zhang Y H, Zhu B J, Zhang Z, Li Y T, Armstrong C, Zemaityte E, Bradford P, *et al.* 2020 *Phys. Rev. X* **10** 031062
[25] Kuratov A S, Brantov A V, Aliev Y M and Bychenkov V Y 2016 *Quantum Electron.* **46** 1023
[26] Herzer S, Woldegeorgis A, Polz J, Reinhard A, Almassarani M, Beleites B, Ronneberger F, Grosse R, Paulus G G, Hübner U, May T and Gopal A 2018 *New J. Phys.* **20** 063019
[27] Garibian G M 1958 *Soviet Journal of Experimental and Theoretical Physics* **6** 1079
[28] Zheng J, Tanaka K A, Miyakoshi T, Kitagawa Y, Kodama R, Kurahashi T and Yamanaka T 2003 *Phys. Plasmas* **10** 2994
[29] Schroeder C B, Esarey E, van Tilborg J and Leemans W P 2004 *Phys. Rev. E* **69** 016501
[30] Macchi A, Borghesi M and Passoni M 2013 *Rev. Mod. Phys.* **85** 751
[31] Rusby D R, Armstrong C D, Scott G G, King M, McKenna P and Neely D 2019 *High Power Laser Science and Engineering* **7** e45
[32] Link A, Freeman R R, Schumacher D W and Van Woerkom L D 2011 *Phys. Plasmas* **18** 053107
[33] Jin Z, Zhuo H B, Nakazawa T, Shin J H, Wakamatsu S, Yugami N, Hosokai T, Zou D B, Yu M Y, Sheng Z M and Kodama R 2016 *Phys. Rev. E* **94** 033206
[34] Woldegeorgis A H, Beleites B, Ronneberger F, Grosse R and Gopal A 2018 *Phys. Rev. E* **98** 061201
[35] Gopal A, Woldegeorgis A, Herzer S and Almassarani M 2019 *Phys. Rev. E* **100** 053203
[36] Woldegeorgis A, Herzer S, Almassarani M, Marathapalli S and Gopal A 2019 *Phys. Rev. E* **100** 053204
[37] Cai J, Shou Y, Geng Y, Han L, Xu X, Wen S, Shen B, Yu J and Yan X 2023 *High Power Laser Science and Engineering* **11** e90
[38] Liao G Q and Li Y T 2019 *IEEE Trans. Plasma Sci.* **47** 3002
[39] Daido H, Nishiuchi M and Pirozhkov A S 2012 *Rep. Prog. Phys.* **75** 056401

[40] Pukhov A and Meyer-ter Vehn J 1996 *Phys. Rev. Lett.* **76** 3975

[41] Derouillat J, Beck A, Pérez F, Vinci T, Chiaramello M, Grassi A, Flé M, Bouchard G, Plotnikov I, Aunai N, *et al*. 2018 *Comput. Phys. Commun.* **222** 351

[42] Bussolino G, Faenov A, Giulietti A, Giulietti D, Koester P, Labate L, Levato T, Pikuz T and Gizzi L 2013 *J. Phys. D: Appl. Phys.* **46** 245501

[43] Falk K, Šmíd M, Boháček K, Chaulagain U, Gu Y, Pan X, Perez-Martin P, Krůs M and Kozlová M 2023 *Sci. Rep.* **13** 4252

[44] Ma W 2023 *Nano Res.* **16** 12572

[45] Wang P, Qi G, Pan Z, Kong D, Shou Y, Liu J, Cao Z, Mei Z, Xu S, Liu Z, *et al.* 2021 *High Power Laser Science and Engineering* **9** e29

[46] Pan Z, Liu J, Wang P, Mei Z, Cao Z, Kong D, Xu S, Liu Z, Liang Y, Peng Z, Xu T, Song T, Chen X, Wu Q, Zhang Y, Han Q, Chen H, Zhao J, Gao Y, Chen S, Zhao Y, Yan X, Shou Y and Ma W 2024 *Phys. Plasmas* **31** 043108

[47] Pak T, Rezaei-Pandari M, Kim S B, Lee G, Wi D H, Hojbota C I, Mirzaie M, Kim H, Sung J H, Lee S K, *et al*. 2023 *Light: Science & Applications* **12** 37

[48] Ishak B 2018 *Contemporary Physics* **59** 308

[49] Krainara S, Chatani S, Zen H, Kii T and Ohgaki H 2018 *J. Phys.: Conf. Ser.* **1067** 032022

[50] Green B, Kovalev S, Asgekar V, Geloni G, Lehnert U, Golz T, Kuntzsch M, Bauer C, Hauser J, Voigtlaender J, *et al*. 2016 *Sci. Rep.* **6** 22256

[51] Krasilnikov M, Aboulbanine Z, Adhikari G, Aftab N, Asoyan A, Boonpornprasert P, Davtyan H, Georgiev G, Good J, Grebinyk A, *et al*. 2025 *Phys. Rev.: Accelerators and Beams* **28** 030701

[52] Ulbricht R, Hendry E, Shan J, Heinz T F and Bonn M 2011 *Rev. Mod. Phys.* **83** 543

[53] Kleine-Ostmann T and Nagatsuma T 2011 *Journal of Infrared, Millimeter, and Terahertz Waves* **32** 143

[54] Riccardi E, Pistore V, Kang S, Seitner L, De Vetter A, Jirauschek C, Mangeney J, Li L, Davies A G, Linfield E H, *et al*. 2023 *Nat. Photon.* **17** 607

[55] Couture N, Lippl M, Cui W, Gamouras A, Joly N Y and Ménard J M 2024 *Phys. Rev. Appl.* **21** 054020

[56] Fill E E 2001 *Phys. Plasmas* **8** 4613

[57] Zhang Y, Wang C, Huai B, Wang S, Zhang Y, Wang D, Rong L and Zheng Y 2020 *Appl. Sci.* **11** 71

[58] Damyanov D, Batra A, Friederich B, Kaiser T, Schultze T and Balzer J C 2020 *IEEE Access* **8** 151997

[59] Pan Z, Liu J, Wang P, Mei Z, Cao Z, Kong D, Xu S, Liu Z, Liang Y, Peng Z, Xu T, Song T, Chen X, Wu Q, Zhang Y, Han Q, Chen H, Zhao J, Gao Y, Chen S, Zhao Y, Yan X, Shou Y and Ma W 2024 *Phys. Plasmas* **31** 043108